PORE CHARACTERISTICS AND ELECTROCHEMICAL PERFORMANCE OF ACTIVATED CARBON FIBERS FOR ELECTRIC DOUBLE-LAYER CAPACITORS

Yong-ming Tian[1,2], Yan Song[*1], Xi-miao Liu[3], Rui Zhang[3], Quan-gui Guo[1], Lang Liu[1]

[1.] *Key Laboratory of Carbon Materials, Institute of Coal Chemistry, Chinese Academy of Sciences, Taiyuan, Shanxi, 030001, P. R. China*

[2.] *Graduate University of Chinese Academy of Sciences, Beijing, 100039, P.R. China.*

[3.] *State Key Laboratory of Chemical Engineering, East China University of Science and Technology, Shanghai, 200237, China*

* Corresponding author, Tel:+86-351-4250553; Fax: +86-351-4083952; E-mail: aic00@sina.com.cn、yansong@126.com

Abstract

A series of pitch-based activated carbon fibers (ACFs), including micro- (from OG5A to OG20A) and mesoporous (MP60 and MP90) ACFs, were used as electrode materials in 1.0M Et_4NBF_4/PC electrolyte for electric double layer capacitors (EDLC). The relationship between the capacitances of carbon electrodes and their pore characteristics was demonstrated in detail. The results showed that the gravimetric capacitance C_g increased with the increase of surface area in general for all the samples investigated. However, the capacitance not only depended on the surface area, but also on the pore size distribution. The capacitance of samples (OG5A and OG7A) with small pore size was very low for the ion-sieving effect, and the surface capacitance for all the samples increased with the increase of mesopore fraction.

***Keyword**:* activated carbon fibers; capacitance; ac impedance; pore size distribution

1 Introduction

Electric double-layer capacitors (EDLCs) are unique electrical storage devices, which can store more energy than conventional capacitors and offer much higher power density than batteries. In resent years, several studies have suggested promising properties of activated carbons when used in EDLCs systems, but the absence of a systematic analysis does not allow a reliable correlation between the structural characteristics of the materials and their capacitance behaviors. Hence, understanding the certain relationship is very important for the design of carbon electrodes and electrochemical capacitors with

improved performances. As can be seen from some literatures, though the high total surface area is a leading requirement for the electrode material, some other respects such as the proper pore size distribution and surface structure are also very important [1-6].

For one thing, it is the pore size distribution and surface wettability that determine the accessibility of the porous system to a given electrolyte. On the other hand, specific capacitance of an activated carbon (AC) is also strongly dependent on the electrolyte characteristics and properties, such as the ions dimensions, the dielectric constant, the solvating power and the viscosity. Capacitance of a carbon-based capacitor also results from conductivity of the carbon-binder composite, thickness of the composite, suitable separator and so on. As a result, the charge accumulated in a mass (or volume) unit of a practical porous material varies widely from one activated carbon to another [7].

It has been shown that sometimes activated carbons can lead to gravimetric capacitances as high as 300 Fg^{-1} for aqueous H_2SO_4 or KOH electrolytes. However, various studies [8-12] have pointed out the limitations of these materials for high power applications. For example, it has been reported that ionic motion may be hindered in narrow nanopores, which will reduce the rate of energy delivery. Furthermore, in the case of non-aqueous electrolytes such as $(C_2H_5)_4NBF_4$ in CH_3CN, both charge storage and energy delivery rates can be limited by the size of the ions [9,13-15]. It is therefore believed that the electrochemical performance of activated carbons with much more mesopores could be more superior in application.

In present work, a series of pitch-based commercial ACFs(some kinds with more than fifty percent of mesopores) were investigated in 1M Et_4NBF_4/PC electrolyte. The relationship between electrochemical performance and porous structure characteristics was elucidated on the basis of pore characteristics investigation of these ACFs .

2 Experimental

2.1 Materials

Picth-based activated carbon fibers (ACFs) (provided by Osaka Gas Company) with different pore structure, including OG5A, OG7A, OG10A, OG15A, OG20A, MP60 and MP90, were used in this study.

2.2 Porosity Measurement

Porous texture of ACFs was characterized by nitrogen adsorption at 77K using Micromeritics ASAP-2000 instrument. The pore size distribution curve was calculated by the DFT (density functional theory) method. Pore diameter (D) was referred to the pore size value corresponding to the peak position in pore size distribution curve. The specific surface areas (S_{BET}) were calculated from the adsorption data in the relative pressure interval from 0.04–0.2 using the Brunauer–Emmett–Teller (BET) method. The total pore volume (V_{total}) was estimated from the amount adsorbed at a relative pressure of 0.98. The Dubinin–Radushkevich (DR) theory was employed for estimating the micropore volume (V_{mic}) [16], and mesopore volume (V_{mes}) was calculated from the balance of V_{total} and V_{mic}. From α_s-plot, microporous surface area S_{mic} [17,18] was determined, and mesoporous surface area S_{mes} was obtained from the balance of S_{BET} and S_{mes}. Mesopore fraction was calculated from V_{mes}/V_{total}.

2.3 EDLC capacitance measurements

The sheet-type electrodes about 400-500μm in thickness were prepared by mixing activated carbon fibers (80 mass%) and graphite (10 mass %) with polytetrafluoroethylene (PTFE) binder (10 mass %), kneading and then rolling to a thin sheet. A cellulose separator with the thickness of 40μm was sandwiched with a pair of the sample sheets to form electrodes. The capacitance of the sample electrode was determined by two electrode system without reference electrode using the test cell. The electrolyte was 1M Et_4NBF_4/PC electrolyte. The dryness of all components of the cell (test sheets, separators, containers, etc.) and the process of assembled cell impregnated with an electrolyte solution were under vacuum and kept in a glove box. The galvanostatic charge/discharge capacitance (C_g) of electrode was measured using a Program Testing System (produced by Wuhan Lixing Co. Ltd., China). Charge and discharge voltages were ranged between 3 and 0 V. The C in Farad was calculated on the basis of [1]:

$$C = (I\Delta t)/\Delta V \qquad (1)$$

where C was the capacitance, I was the constant discharge current (value of discharge current is 2mA in this study),Δt was the discharge time, and ΔV was the potential range. For each sample, at least three electrodes were assembled and measured. The specific capacitance shown in Table 2 was the average value of the measurement results. The specific capacitance C_g was expressed as $F.g^{-1}$ of carbon electrode material. The surface capacitance C ($F.cm^{-2}$) was defined as the gravimetric specific capacitance ($F.g^{-1}$) divided by BET surface area.

Gamry Instrument (USA) was used to measure impedance of the electrodes. The ac impedance measurements were carried out at 300mV in the frequency range from 100 kHz to 5 mHz and the ac amplitude was 5mV.

3 Results and discussion

3.1 Pore characteristics of the carbon materials

Fig. 1 showed the adsorption/desorption isotherms of nitrogen for all the samples. The adsorption/desorption isotherms of OG5A, OG7A, OG 10A, OG15A and OG20A gave a typical type I isotherms [19], suggesting the presence of micropores. While MP60 and MP90 were all representative of type □ shapes, which could be observed by the very large hysteresis loop, indicating a considerable amount of mesopores in the ACFs. The porous structure parameters of carbonaceous materials were listed in Table 1. It can be observed that this series of samples covered a very wide range of surface areas (BET surface area from 445 up to 1862 m^2/g). At the same time, the mesopore fraction of MP60 and MP90 reached about 70%.

Fig. 2 showed the pore size distributions of all the samples. It was clearly seen that these ACFs had apparently different pore size distribution. OG5A and OG7A centralized the pore width mainly in 0.7nm and 0.6nm, respectively. This kind of narrow pore size distribution may have beneficial impact on the capacitance performance in aqueous solution, as reported in some other literatures. However, it seemed that this kind of pore structure was insufficient to form electronic double layer between the non-aqueous electrolyte and electrodes (see Table 2). The pore size distribution of OG 10A, OG15A and OG20A was very similar, and the pore size appeared three peaks at about 0.8nm, 1.2nm and 2nm. MP60 and MP90 presented nearly the same pore systems with size centered at 0.6 nm and 1.2 nm,

while the former with a marked peak distribution at 3.4 nm and that of the latter centralizing in 5nm in mesopores, which may result in the different electrochemical characterization in the following details.

3.2 Relationship between double layer capacitance and surface area

In general, it is believed that there was a direct relationship between the BET surface area and the double layer capacitance (DLC) of porous carbons [20,21]. Theoretically, the higher the specific surface area of an activated carbon, the higher the specific capacitance should be expected. Practically, the situation was more complicated.

Table 2 listed the capacitance values of all the samples. From Table 2, it can be observed that the ACFs with relative lower surface area (OG5A and OG7A) had a very low capacitance, much lower than the expected value according to the trend obtained from other microporous ACFs (OG10A、OG15A and OG20A), no matter the value of gravimetric specific capacitance or surface capacitance. The entry of the electrolyte was very difficult for the small pore size of OG 5A and OG7A, so the capacitance of these two samples was very low compared with other samples. The very small micropores (non-accessible pores) did not contribute to the total double layer capacitance of the sample. This so-called ion-sieving effect [22] had also been observed by other authors using other materials and electrolytes [1,23].

Fig. 3 presented the values of gravimetric capacitance versus the BET specific surface area (S_{BET}). The nearly linear relationship between the gravimetric capacitance C_g and S_{BET} of the samples suggested that the capacitance was controlled primarily by the surface area.

Moreover, it is interesting to note that an obvious deviation from the C_g-S_{BET} linear relationship in Fig. 3 was observed, which represented the performance of MP60 and MP90 in reality.Though with lower specific surface area compared with OG20A, their galvanostatic specific capacitance could be comparable. This phenomenon might be ascribed to the different pore structure.

3.3 Correlation between double layer capacitance and pore structure

It is well known that EDLC electrode materials should not only have a large surface area for charge accumulation, but also have an appropriate pore structure for electrolyte wetting and rapid ionic motion [24,25].

Shi [7], who used C_{mic} and C_{mes} to express the surface capacitance, proposed to understand the observed capacitance of EDLCs by assuming different contributions of different surfaces. So surface capacitance was employed (see Table 2) here to represent the contribution of specific surface area to capacitance and C_{mes}/C was also used here, to express distribution of mesopores. From Table 2, it can be seen that the performance of OG5A and OG7A can be mainly attributed to the micropores, while mesopores showed nearly 40 percent the effect to that of OG10A, OG15A and OG20A, respectively. OG20A had bigger value of gravimetric specific capacitance than OG15A and OG10A, though with the similar pore size distribution discriminating only in some mesopores. As concluded from Fig. 3 and the value of mesopore fraction and C_{mes}/C, it indicated that not only the biggest surface area but also wider mesopores of OG20A played an important role.

It is interesting to note from Fig. 4 that an approximately obvious linear relationship of mesopore fractions versus surface capacitance could be observed, that is, the surface capacitance basically increased with the growing majority of mesopore fraction for all the ACFs samples. As mentioned above, the specific surface area of MP90 and OG20A were 1144 m^2g^{-1} and 1862m^2g^{-1}, respectively.

However, the surface capacitance of MP90 was 10μFcm^{-2}, which was the biggest value among all the samples studied. In consideration of it's most majority of mesopore fractions, it seemed that the suitable amount of mesopores ensured a rapid mass transport of ions within the electrode facilitating the charging and discharging the double layer, and resulted in better capacitance performance subsequently. From the study, it was available to extend the mesopore fraction in order to obtain the higher surface capacitance, at least to the present ACFs, based on the same carbon precursor.

3.4 Performance of Electrochemical impedance

Ac impedance spectroscopy, which distinguished the resistance and capacitance of devices, was further employed to analyze the performance of the capacitor cells. Fig. 5 depicted the standard Nyquist plots of the ACFs for scans at different potentials. The complex plane consisted of a small semicircle at high frequencies (bulk RC response) followed by a vertical spike at low frequency region indicating the pure double layer capacitive (C_{dl}) behavior[26].The semi-circle in the high frequency region represented the impedance at the interface between the current collector and the carbon electrode as well as that between the carbons [27,28]. In the low frequency region, the vertical line exhibited the domination of the capacitive behavior at the electrolyte and carbon interface.

The diameter of the semicircle reflected the the interface resistance of the electrochemical cells. From Fig.5, it can be found that the order of the interface resistance of the samples was as followed: OG20A<OG7A<OG5A<MP60<OG10A<OG15A<MP90. At the same time, the electrochemical cell composed of OG20A appeared better capacitive behavior for it possessed relatively perpendicular line to the real part impendance.

Distributed-capacitance effect of porous electrodes may originate partially from a non-uniform charging rate distribution through the porous electrode (i.e. the exterior surface of the porous electrode charged or discharged at a faster rate than the interior) as a result of an ohmic resistance along the path of the pores [29-31]. Generally speaking, the ohmic resistance should be small in the porous electrodes of the present work, since no obvious transition zone between the semi-circle and the linear part was observed in the Nyquist plot, except that of OG5A and OG7A. This may be attributable to the short path of micropores in ACFs [32].

4 Conclusions

The electrochemical performance of ACFs with different pore structure in 1M Et_4NBF_4/PC electrolyte was investigated. The results showed that gravimetric capacitance C_g increased with surface area, reaching a maximum of 119F/g for a surface area of 1862m^2/g (OG20A). At the same time, the results confirmed that capacitance not only depended on the surface area, but also on the pore size distribution. The effect of pore size distribution had been observed as followed: First of all, capacitance was higher for the sample with wider pore size than for the samples (OG5A and OG7A) with too narrow micropore size. The existence of a very small pore made the entry of the Et_4NBF_4/PC electrolyte into the pores difficult. Then, the non-accessible pores do not contribute to total double layer capacitance. Secondly, the capacitance was higher for a sample with wider pore size distribution (MP90) than for a sample with higher surface area but narrow pore size distribution (OG10A). Finally, an obvious linear shape between mesopore fraction and surface capacitance was shown for all the

ACFs samples. From the study, it was available to extend the mesopore fraction in order to obtain the higher surface capacitance, at least to the present ACFs, based on the same carbon precursor.

5 Acknowledgements

This work was supported by Fund of 863 Project of China (2006AA11A166), Fund of Nature Science Foundation of China (50602046) and Fund of ICC, and CAS (Institute of Coal Chemistry, Chinese Academy of Sciences) for Youth.

6 References

[1] D. Qu, H. Shi, J. Power Sources 74 (1998) 99.

[2] E. Frackowiak, F. Béguin, Carbon 39 (2001) 937.

[3] G. Salitra, A. Soffer, L. Eliad, Y. Cohen, D. Aurbach, J. Electrochem. Soc. 147 (2000) 2486.

[4] G. Gryglewicz, J. Machnikowski, E. Lorenc-Grabowska, G. Lota, E. Frackowiak, Electrochim. Acta 50 (2005) 1197.

[5] A. Braun, M. B¨artsch, B. Schnyder, R. K¨otz, O. Haas, H.-G. haubold, G. Goerigk, J. Non-Cryst. Solids 260 (1999) 1.

[6] O. Barbieri, M. Hahn, R. K¨otz, Carbon 43 (2005) 1303.

[7] H. Shi, Electrochim. Acta 41 (1996) 1633.

[8] J.S. Noh, J.A. Schwarz, Carbon 28 (1990) 675.

[9] M. Endo, T. Maeda, T. Takeda, Y.J. Kim, K. Koshiba, H. Hara, M.S. Dresselhaus, J. Electrochem. Soc. 148 (2001) A910.

[10] K. Kinoshita, Carbon: Electrochemical and Physicochemical Properties (Ch. 3, 5 and 6), Wiley, New York, 1987.

[11] J.R. Macdonald, D.R. Franceschetti, in: J.R. Macdonald (Ed.), Impedance Spectroscopy: Emphasizing Solid Materials and Systems (Ch. 2), Wiley, New York, 1987.

[12] I. Tanahashi, A. Yoshida, A. Nishino, J. Electrochem. Soc. 137 (1990) 3052.

[13] T. Pajkossy, T. Wandlowski, D.M. Kolb, J. Electroanal. Chem. 414 (1996) 209.

[14] T. Pajkossy, Solid State Ionics 94 (1997) 123.

[15] H.-K. Song, Y.-H. Jung, K.-H. Lee, L.H. Dao, Electrochim. Acta 44 (1999) 3513.

[16] M. Hahn, M. B¨artsch, O. Barbieri, J.-C. Sauter, R. K¨otz, R. Gallay, Electrochem. Solid-State Lett. 7 (2) (2004) A33.

[17] M. Inagaki, T. Suwa, Mol. Cryst. Liq. Cryst. 386 (2002) 197.

[18] Gra˙zyna Gryglewicz, Jacek Machnikowski, Ewa Lorenc-Grabowska, Grzegorz Lota, Electrochim. Acta. 50 (2005) 1197

[19] C. Vix-Guterl, E. Frackowiak, K. Jurewicz, M. Friebe, J. Parmentier, F.Beguin, Carbon 43 (2005) 1293.

[20] T. Osaka, X. Liu, M. Nojima, T. Momma, J. Electrochem. Soc. 146 (1999) 1724.

[21] D. Lozano-Castello´, D. Cazorla-Amoro´s, A. Linares-Solano, Carbon 41 (2003) 1765–1775

[22] Salitra G, Soffer A, Eliad L, Cohen Y, Aurbach D, J Electrochem Soc 2000;147(7):2486–93.

[23] T. Momma, X. Liu, T. Osaka, Y. Ushio, Y. Sawada, J. Power Sources 60 (1996) 249.

[24] X. Liu, T. Osaka, J. Electrochem. Soc. 143 (1996) 3982.

[25] O.B. Yang, J.C. Kim, J.S. Lee, Y.G. Kim, Ind. Eng. Chem. Res. 32 (1992) 1692.

[26] Y.-R Nian, H. Teng, J. Electroanal. Chem. 540 (2003) 119.
[27] X. Liu, T. Osaka, J. Electrochem. Soc. 143 (1996) 3982.
[28] T. Momma, X. Liu, T. Osaka, Y. Ushio, Y. Sawada, J. Power Sources 60 (1996) 249.
[29] L.G. Austin, E.G. Gagnon, J. Electrochem. Soc. 120 (1973) 251.
[30] X. Liu, T. Osaka, J. Electrochem. Soc. 144 (1997) 3066.
[31] S. Yoon, J. Lee, T. Hyeon, S.M. Oh, J. Electrochem. Soc. 147 (2000) 2507.
[32] S. Yoon, J. Lee, T. Hyeon, S.M. Oh, J. Electrochem. Soc. 147 (2000) 2507.

Table 1 Pore structure of ACFs

Activated carbons	S_{BET} (m^2g^{-1})	S_{mic} (m^2g^{-1})	S_{mes} (m^2g^{-1})	V_{mic} (cm^3g^{-1})	V_{mes} (cm^3g^{-1})	V_{total} (cm^3g^{-1})	Mesopore fraction (%)
OG5A	654	618	36	0.27	0.04	0.31	12.9
OG7A	445	407	38	0.19	0.03	0.22	13.6
OG10A	1646	954	692	0.39	0.51	0.90	56.7
OG15A	1604	921	683	0.37	0.44	0.81	54.3
OG20A	1862	1138	724	0.47	0.50	0.97	51.5
MP60	1195	741	454	0.29	0.65	0.94	69.1
MP90	1144	682	462	0.27	0.83	1.10	75.5

Table 2 Capacitance values for all samples

Activated carbons	C_g (Fg^{-1})	Et_4NBF_4/PC C (μFcm^{-2})	C_{mic} (μFcm^{-2})	C_{mes} (μFcm^{-2})	C_{mes}/C (%)
OG5A	8	1.2	1.1	0.1	8.3
OG7A	3.5	0.8	0.7	0.1	12.5
OG10A	98	6	3.5	2.5	41.7
OG15A	112	7	4.0	3.0	42.9
OG20A	119	6	3.7	2.3	38.3
MP60	100	8	5.0	3.0	37.5
MP90	111	10	6.0	4.0	40.0

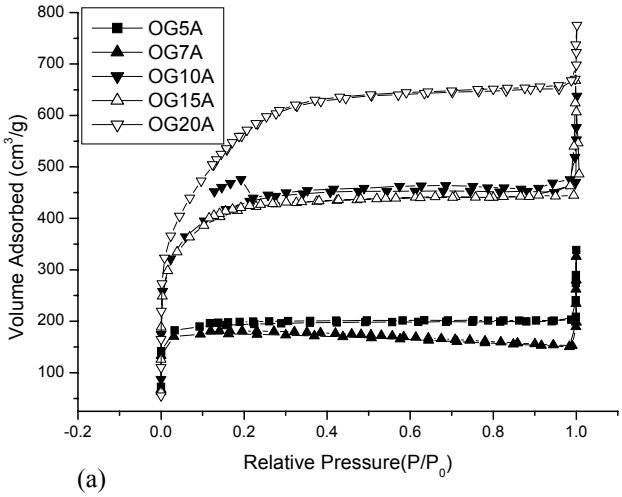

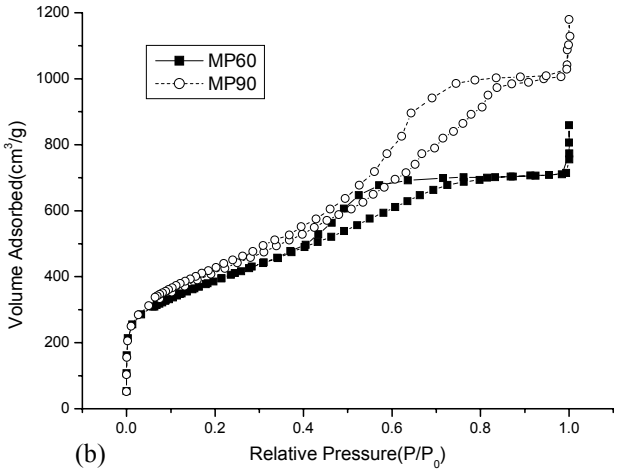

(a) microporous ACFs; (b) MP60 and MP90.

Figure. 1 Nitrogen adsorption/desorption isotherms of samples.

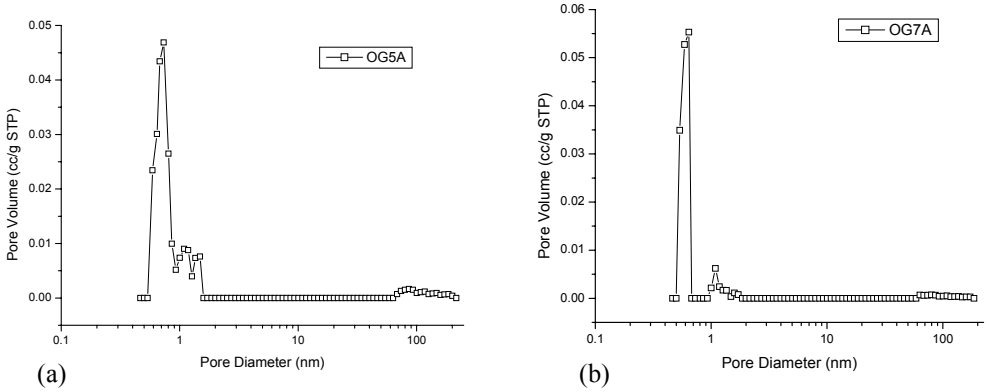

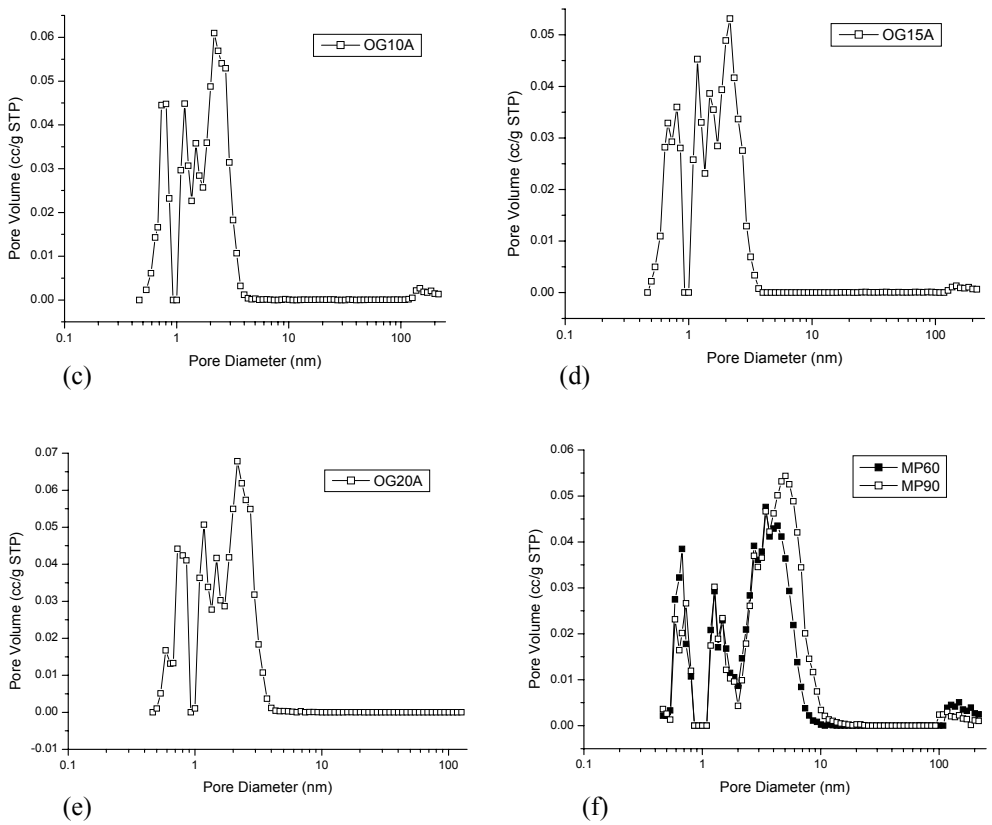

(a) OG5A (b) OG7A (c) OG10A (d) OG15A (e) OG20A(f) MP60 and MP90.

Figure 2 Pore size distributions of samples

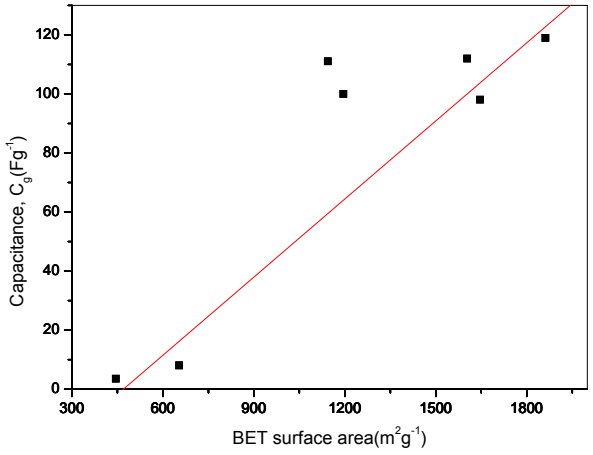

Figure. 3 Specific capacitance as a function of BET surface area for ACFs.

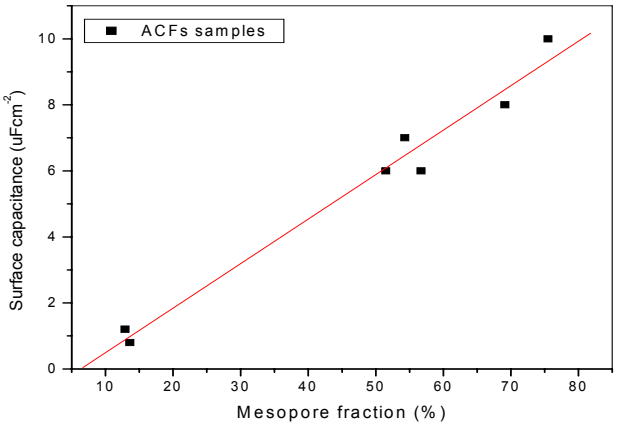

Figure 4 Relationship between mesopore fractions and surface capacitance for all samples

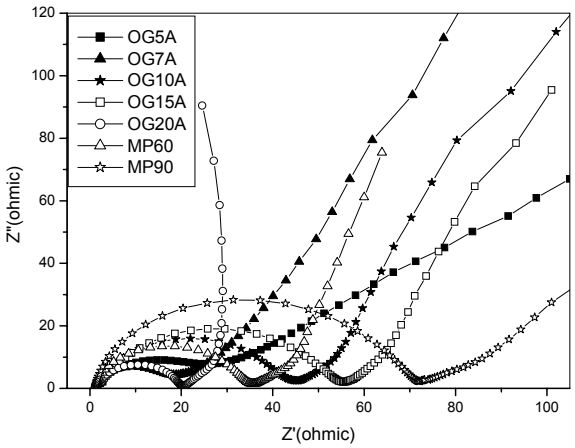

Figure 5 Nyquist impedance spectra of ACFs